


Replication / Neuroscience

# [Re] Spread of alpha-synuclein pathology through the brain connectome is modulated by selective vulnerability and predicted by network analysis

Thomas E. Paul<sup>1,2</sup> and Mathieu Bourdenx<sup>1,2</sup> <sup>1</sup>Univ. de Bordeaux, Institut des Maladies Neurodégénératives, UMR 5293, Bordeaux, France – <sup>2</sup>CNRS, Institut des Maladies Neurodégénératives, UMR 5293, Bordeaux, FranceEdited by  
(Editor)Received  
01 November 2018Published  
–DOI  
–

## 1 Introduction

Parkinson's disease (PD) is a common motor neurodegenerative disorder, characterized in part by the progressive loss of pigmented dopaminergic neurons from the *Substantia Nigra pars compacta*. The main neuropathological hallmark of PD is the progressive accumulation of  $\alpha$ -synuclein in fibrillar aggregates named Lewy Bodies (in the soma) or Lewy Neurites (in neurites) [1]. Interestingly, Lewy pathology follows a predictable pattern of progression in the brain suggesting that  $\alpha$ -synuclein can propagate from neurons to neurons [2]. Such observation, common to many neurodegenerative diseases [3], prompted initiatives to model and predict pathology progression in the brain of patients with neurodegenerative disorders.

In 2012, Raj and colleagues developed a Network Diffusion Model (NDM) to predict atrophy progression in dementia [4]. For this purpose, they compared Magnetic Resonance Imaging recordings from healthy young subjects, healthy old subjects, and old patients suffering from either Frontotemporal Dementia or Alzheimer's Disease. Their study suggested that patterns of atrophy within the dementia spectrum could be explained by transmission of the disease along neuronal pathways. Using their model, they demonstrated a path for predicting future atrophy in individuals starting from baseline. The NDM model was later applied to other diseases using various kind of data. In 2017, Mezas and Raj showed that the spread of amyloid- $\beta$  pathology, involved in Alzheimer's disease, in mice was driven by spatial proximity but not network connectivity [5]. At the opposite, progression of tau pathology, also involved in Alzheimer's disease and other tauopathies, was better recapitulated by connectivity [6]. In 2019, Henderson and colleagues reported that progression of  $\alpha$ -synuclein pathology, similar to tau pathology, is largely predicted by anatomical connectivity between brain structures [7].

We here replicated the core of the NDM applied to  $\alpha$ -synuclein spread in mice as implemented by Henderson and colleagues [7]. R scripts, connectivity matrix and experimental datasets were made fully accessible by the authors on GitHub allowing an easy process. We were able to reproduce qualitatively and quantitatively the main results of the paper. The aim of the present replication is not to fully replicate the entire paper but to focus on the core model and immediate results (shown in Figures 4 and 5 in the original paper).

Copyright © 2021 T.E. Paul and M. Bourdenx, released under a Creative Commons Attribution 4.0 International license.  
Correspondence should be addressed to Mathieu Bourdenx (mathieu.bourdenx@u-bordeaux.fr)  
The authors have declared that no competing interests exist.

## 2 Background

### 2.1 Graph Theory and brain connectivity

Henderson et al. combined quantitative pathology mapping in the mouse brain with network modeling to understand the spatiotemporal pattern of spread of  $\alpha$ -synuclein pathology [7]. Graph theory is a branch of mathematics applicable to Neuroscience. The brain is a complex system that can be modeled as a network or graph. When applied properly, Graph theory can offer important insights into different aspects of brain networks such as architecture, evolution, development, or clinical disorder [8].

Networks are defined as a collection of elements (or nodes) and their pairwise links (or edges) that can be summarized in the form of a connectivity matrix (named adjacency matrix). Depending on the type of graph, edges can have binary values (present: 1 - absent: 0) or actual weights reflecting connection strength. A graph is called undirected when an edge  $e$  reciprocally connects nodes  $V_a$  and  $V_b$ . Conversely, a graph is named directed when the edge  $e$  is projecting from  $V_a$  to  $V_b$  but not from  $V_b$  to  $V_a$ .

Thanks to the initiative from the Allen Institute for Brain Science's Mouse Connectivity Atlas (MCA), the mouse brain mesoscale connectome is now freely accessible for the neuroscience community [9]. In a matrix, connectivity is represented as "outgoing" along rows and "incoming" along columns. From the adjacency matrix, the in-degree and out-degree distributions can be computed as respectively the sum of all entries in the corresponding row and the sum of all entries in the corresponding column and are represented in diagonal matrices.

The Laplacian graph is a matrix used to explore the properties of a network. It is computed using the adjacency matrix and either the in-degree or out-degree graph depending on the applications.

### 2.2 Model description

The model used by Henderson et al. requires the mouse brain connectome (discussed in the previous section) and whole brain  $\alpha$ -synuclein pathology quantification.

The experimental model of  $\alpha$ -synuclein pathology propagation used in the study is the classical  $\alpha$ -synuclein pre-formed fibrils (PFFs -  $5\mu\text{g}$ ) unilateral injection in the dorsal striatum of non-transgenic mice (NTG) [10, 7]. Following inoculation, NTG mice were terminated at 3, 6, or 9 months post-injection (MPI). Brain pathology was assessed using traditional immunohistochemical methods to detect pathological  $\alpha$ -synuclein phosphorylated on Serine129 (pS129). Quantification (as percent of region occupied by immunostaining) was performed on both brain hemispheres (ipsilaterally and contralaterally to the injection point) in 58 different regions. Thus, the pathology dataset provided by the authors on their repository is an Excel sheet with values for 5 mice per group and time-point for all 116 brain regions.

Using the dataset from [9] for synaptic connection, the authors generated a directed and weighed connectivity graph  $G = V, E$  whose nodes  $V$  are  $N$  cortical and subcortical grey matter regions and whose edges  $e_{ij} \in E$  represent an axonal projection from  $V_i$  to  $V_j$ . They then defined the weighed adjacency matrix of  $G$  as  $A = [A_{ij}]$  generating a final parcellation of 116 regions.

The magnitude of observed  $\alpha$ -synuclein pathology of all  $N$  nodes at a time  $t$  is the vector  $x_t$ . The predicted regional  $\alpha$ -synuclein pathology  $\hat{x}_t$  is a function of the adjacency matrix  $A$  and a seed region  $seed \in E$  and is computed as shown in (1):

$$\hat{x}_t = e^{-cLt} x_o \quad (1)$$

Where:

- $c$  is a constant designed to achieve an optimal match with the data as the empirical diffusion constant for the pathology is *a priori* unknown.
- $t$  stands for the timepoint of the prediction.
- $L$  is the out-degree Laplacian matrix computed as shown in (2):

$$L_{ij} = \begin{cases} -A_{ij} & \text{for } i \neq j \\ \sum_{j=1}^N A_{ij} & \text{for } i = j \end{cases} \quad (2)$$

- $x_0$  is the seed vector computed as shown in (3):

$$x_0 = \begin{cases} 0 & \text{for } i \neq seed \\ 1 & \text{for } i = seed \end{cases} \quad (3)$$

### 3 Material and Methods

Henderson et al. coded their model using R and MATLAB. Codes and dataset were made fully accessible on GitHub by the authors. In order to only rely on opensource and free tools, we decided to reproduce the model in Python 3. We looked for operating systems intercompability and ran our code successfully on both Microsoft Windows 10 and MacOS 11.2.3. **Table1** lists the required packages and their versions. Our code (and the associated datasets) is fully accessible in a GitHub repository <https://github.com/MathieuBo/PathoSpreading>.

Package	Version
NumPy	1.17.0
Pandas	1.1.5
Seaborn	0.11.1
Matplotlib	3.3.2
SciPy	1.5.2
Statsmodels	0.12.1
tqdm	4.7.2

**Table 1.** Description of required packages

## 4 Results

### 4.1 Network model of pathological $\alpha$ -synuclein spread

The model comprises a single free parameter  $c$ , the seed's diffusivity coefficient, that is used to scale the model to experimental results. The model is initiated by creating the seed vector  $x_0$  for the inoculated region: here the caudoputamen (CPu). Then, the

model iterates over possible the values of  $c \in [0, 10]$ . We selected the value of  $c$  that maximizes model fit, defined as the Pearson's correlation  $r$  between  $\log_{10} x_t$  and  $\log_{10} \hat{x}_t$  averaged over all timepoints. **Table 2** summarizes the results including selected  $c$  value and correlation results. Correlation results for each timepoints are also plotted in **Figure 1A-C** (to be compared with Figure4a from the original article). Overall, we obtained a perfect replication, both quantitatively and qualitatively, of the original results.

	Henderson et al.	Replication
Best $c$	1.625	1.625
MPI 1		
Pearson's $r$	0.559	0.559
$p$ -value	$8.085e^{-9}$	$8.085e^{-9}$
MPI 3		
Pearson's $r$	0.696	0.696
$p$ -value	$3.451e^{-17}$	$3.451e^{-17}$
MPI6		
Pearson's $r$	0.648	0.648
$p$ -value	$2.638e^{-14}$	$2.638e^{-14}$

**Table 2. Data correspondence between the reproduced results and the original article.** The results have been rounded up to the third decimal.  $P$ -values for Pearson's correlation tests were corrected for multiple comparisons using Bonferroni's method. MPI: month(s) post injection.

Then, we performed some control experiments on the model to assess its robustness. First, as in the original article, we randomly seeded the diffusion model in all brain regions and calculated the value  $c$ . The 'true' seeded region (CPu) was among the best fits (97th percentile), at each timepoint (**Figure 1D**). Then, we implemented 2 additional controls: we randomly shuffled (over 150 iterations) the connectivity matrix (**Figure 1E**) and the pathology matrix (**Figure 1F**), as in [11]. For each control experiment, we plotted the corresponding value of  $r$ . One can appreciate the profound performance loss in the different control experiments. Our results confirm that the spatiotemporal spread of pathological  $\alpha$ -synuclein is driven by connectivity.

## 4.2 Differential vulnerability of regions is correlated with $\alpha$ -synuclein expression

Intrinsic vulnerability is hypothesized to be a critical factor in the development of brain pathology related to  $\alpha$ -synuclein or other pathogenic proteins [12]. Henderson et al. thought to investigate that aspect using the connectivity-based model. To do so, they used the difference between predicted pathology and observed pathology (i.e. the residues of the linear regression) as a measure of relative vulnerability. Regions with higher pathology than predicted were defined as vulnerable while the ones with lower pathology values than predicted were considered resilient **Figure 2A**. We here present an example at 6 months post-injection **Figure 2B**. We used a 'lollipop' plot to help appreciate the distance to linear regression. Residues presented a bell shape-like distribution centered on 0 **Figure 2C**. We plotted the vulnerability averaged over the 3 timepoints **Figure 2D**. Similarly to the original article, we observed that anterior cortical regions (motor cortex for example), the piriform cortex or the amygdalar region are highly vulnerable.

To determine whether model performance could be improved by the addition of other components, Henderson et al. seek out for factors that could contribute to regional vulnerability. An immediate assumption is that local levels of messenger-RNA (mRNA) encoding for  $\alpha$ -synuclein could influence the future accumulation of  $\alpha$ -synuclein in aggregates. To directly test that hypothesis, the model was modified to account for re-

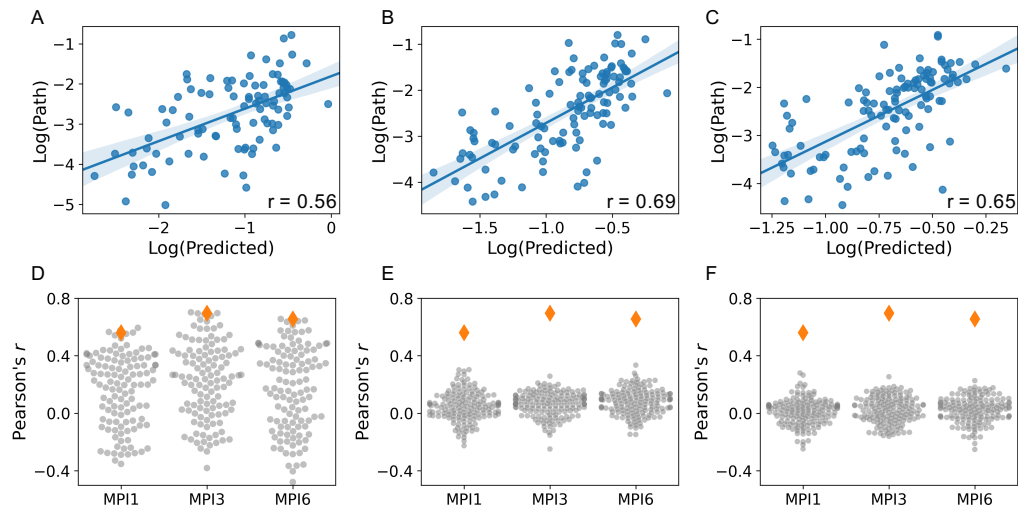


**Figure 1. Network diffusion model based on anatomical connectivity explains pathological  $\alpha$ -synuclein spread.** (A-C) Scatterplots of  $\log_{10}$ (predicted) pathology versus experimentally-measured  $\log_{10}$ (pathology) values at 1 month (A), 3 months (B), and 6 months (C). The blue lines are the linear correlations between experimental and predicted pathology values (shaded areas: 95% confidence interval). Values at the bottom right of each panel are the Pearson's correlation coefficient  $r$  between experimental and predicted pathologies. (D-F) Experimental controls: random seeding in other brain regions (D); shuffle of connectivity matrix (E); and shuffle of pathology matrix (F). For each control experiment, the orange marker represents the actual model fit. MPI: month(s) post injection. Path: experimentally-measured pathology.

gional levels of  $\alpha$ -synuclein mRNA (**Figure 2E**) by directly modifying the adjacency matrix  $A = S \times A$ , where  $S$  is the diagonal matrix of the vector  $R$  containing the regional levels of  $\alpha$ -synuclein mRNA for each brain region of  $A$  such as:

$$S = \begin{cases} R_i & \text{for } i = j \\ 0 & \text{otherwise} \end{cases} \quad (4)$$

Model fitting, performance estimation, etc remained similar.

Incorporation of  $\alpha$ -synuclein expression levels in the network diffusion model improved model performance by up 12% of added explained variance (**Figure 2F-H**). Here also, we perfectly replicated the original results both qualitatively (shown in **Figure 2F-H**) and quantitatively (shown in **Table 3**). Overall, these data suggest that *Snca* gene expression is an important factor impacting the vulnerability of regions and subsequently pathology spread.

### 4.3 In silico seeding of alternative regions

To examine the generalizability of the model, Henderson et al. proceeded to *in silico* seeding of alternative regions such as the Piriform Cortex (Pir) and the Substantia Nigra (SN). **Figure 3** display the pathology spread at 1, 3 and 6 month(s) post-injection after seeding the model with either the Pir or the SN. We successfully obtained similar predictions after seeding in either the Pir or the SN. *In silico* injection in the Pir remarkably corresponds to previous semi-quantitative pathology grading study [14] (**Figure 3A**). On

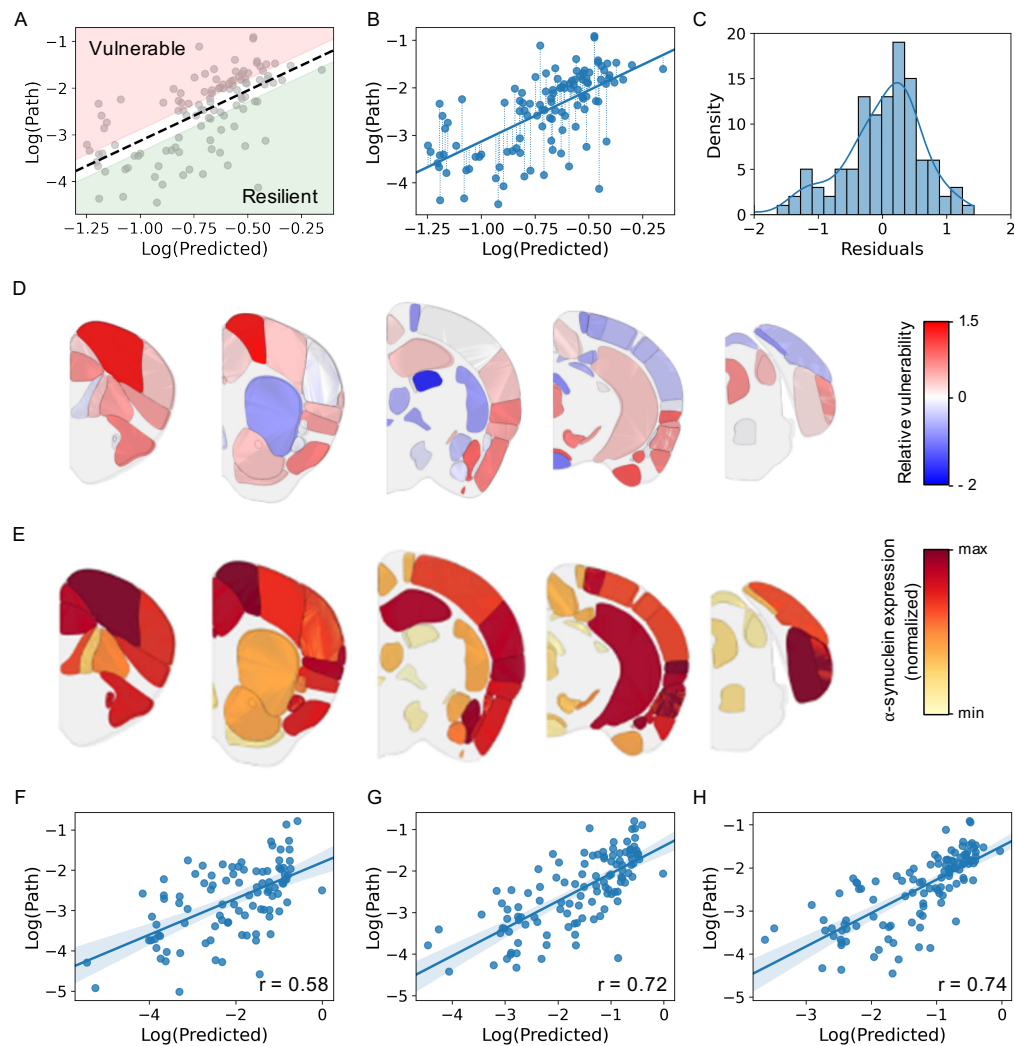


**Figure 2. Differential vulnerability of regions is correlated with  $\alpha$ -synuclein expression.** (A) Conceptual framework for the assessment of regional vulnerability of brain regions. We here show the scatterplot of  $\log_{10}(\text{Predicted})$  and  $\log_{10}(\text{Pathology})$  at 6 months post-injection. The black dashed line is the linear regression between predicted and observed pathologies. The red area indicates brain regions with higher measured pathology than predicted by the model, hence 'vulnerable'. Conversely, the green area indicates brain regions with lower observed pathology than predicted by connectivity, hence 'resilient' brain regions. (B) Example of a lollipop plot for the 6 months timepoint highlighting the distance to the mean linear regression (i.e. residues - dashed blue lines). (C) Distribution of linear regression residues. The solid blue line is the kernel density estimation of the distribution. (D) Heatmap of the residuals between the predicted and measured pathologies plotted on an anatomical mouse brain as a measure of the relative vulnerability of regions averaged over the 3 experimental timepoints, using the *Brainrender* package [13]. (E) Heatmap of the  $\alpha$ -synuclein mean expression energy values obtained from the Allen Brain Atlas *in situ* hybridization study for each of the designated region. Expression was normalized using min/max to ease visualization. Note that Henderson et al. used a divergent colormap to represent a continuous value, hence making it difficult to interpret regional variations. We here chose a sequential continuous colormap to improve the understanding. (F-H) Scatterplots of  $\log_{10}(\text{predicted})$  pathology versus experimentally-measured  $\log_{10}(\text{pathology})$  values at 1 month (F), 3 months (G), and 6 months (H). The blue lines are the linear correlations between experimental and predicted pathology values (shaded areas: 95% confidence interval). Values at the bottom right of each panel are the Pearson's correlation coefficient  $r$  between experimental and predicted pathologies.

	Henderson et al.	Replication
Best $c$	0.414	0.414
MPI 1		
Pearson's $r$	0.580	0.580
$p$ -value	$1.401e^{-9}$	$1.401e^{-9}$
MPI 3		
Pearson's $r$	0.727	0.727
$p$ -value	$2.421e^{-19}$	$2.421e^{-19}$
MPI6		
Pearson's $r$	0.739	0.739
$p$ -value	$2.965e^{-20}$	$2.965e^{-20}$

**Table 3. Data correspondence between the reproduced results and the original article using the model incorporating  $\alpha$ -synuclein mRNA levels.** The results have been rounded up to the third decimal.  $P$ -values for Pearson's correlation tests were corrected for multiple comparisons using Bonferroni's method. MPI: month(s) post injection.

the other hand, *in silico* injection in the SN resulted in slow propagation through the nigrostriatal tract to first the caudoputamen and then to cortical regions (**Figure 3B**). The observed pattern following SN injection mimicks previous experimental results and the staging of human cases [15, 16]. Taken together, these findings support the ability of the Diffusion Network model to generalize data predictions.

## 5 Conclusion

In this article, we successfully replicated the model created by Henderson et al. in Python.

The Network Diffusion Model initially developed by Raj et al. [4] and recently adapted by Henderson et al. [7] is a powerful tool to understand the spread of  $\alpha$ -synuclein pathology. In its initial form the model is solely based on anatomical connectivity between brain regions. Despite its simplicity, the model is able to predict 31% to 47% of the total variance. In a second version, the endogenous  $\alpha$ -synuclein expression (at the mRNA level) is added to the model. The addition improves model performance (up to 12% of added explained variance), although a quantitative analysis should be performed in the future.

Similarly to what is observed in preclinical models of synucleinopathies or in the brain of patients with Parkinson's disease,  $\alpha$ -synuclein pathology is composed of 'islands' of vulnerable neurons susceptible to developing pathogenic protein inclusions. By comparing the pathology observed and predicted based on anatomical connectivity, the model allows to explore regional vulnerability. Finally, seeding in different regions such as the Pir and the SN supports the network diffusion model generalizability. Overall, this model is attractive as it is simple, easily handled, and replicable.

Nonetheless, the model is not without limitations. Other experimental datasets are still required to quantitatively assess the ability of the model to generalize to other seeding regions. Another barrier comes from the available connectivity data [9]. The connectivity matrix used by Henderson et al. and us is at the mesoscale. One implication, for example, is that brain structures are considered homogenous, hence not taking into account the laminar cortical organization for example. The observation of a distinct distribution of the  $\alpha$ -synuclein pathology in cortical layer suggests that lower scale connectivity data could help to capture overlooked events.

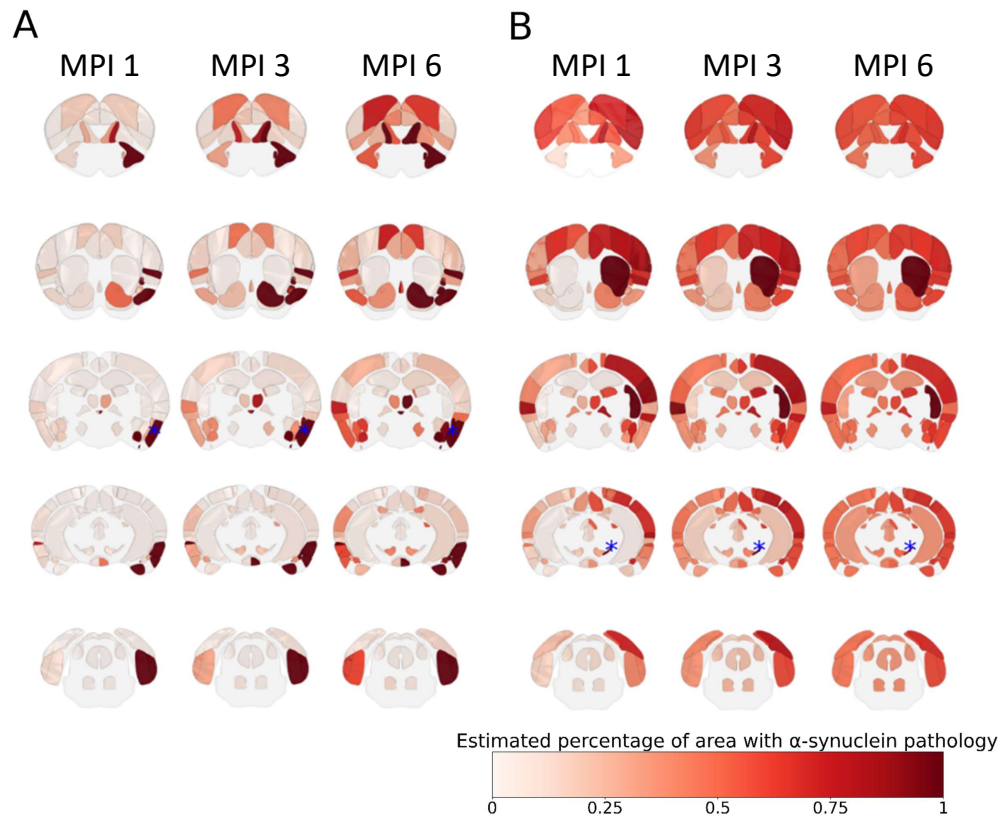


**Figure 3.** *In silico* seeding of alternative regions in the mouse brain Predicted  $\alpha$ -synuclein pathology after *in silico* seeding in the Piriform Cortex (A) or the Substantia Nigra (B) The injection site is indicated on each slice by a blue asterisk. Both Figure A and B are displayed using the *Brainrender* package [13].

Modeling disease propagation in the brain is challenging and often reductionist. Indeed, during disease, the brain changes according at least two parallel processes: the "Dynamics **On** Network" and the "Dynamics **Of** Network" [17]. The first one is related to processes that occur atop a static structure as, for instance,  $\alpha$ -synuclein spread. The second defines the brain network changes over time (e.g. neurodegeneration). A major challenge remains in modeling both these "on" and "of" dynamics. If we were only to understand one dynamic and leave the other dynamic unexplored, we could imagine to still be a step away from the reality of the pathology.

## References

1. B. Dehay et al. "Targeting  $\alpha$ -synuclein for treatment of Parkinson's disease: mechanistic and therapeutic considerations." In: **Lancet Neurol** 14.8 (Aug. 2015), pp. 855–866. doi: 10.1016/S1474-4422(15)00006-X.
2. H. Braak, K. Del Tredici, U. Rüb, R. A. de Vos, E. N. Jansen Steur, and E. Braak. "Staging of brain pathology related to sporadic Parkinson's disease." In: **Neurobiol Aging** 24.2 (2003), pp. 197–211. doi: 10.1016/s0197-4580(02)00065-9.
3. M. Jucker and L. C. Walker. "Propagation and spread of pathogenic protein assemblies in neurodegenerative diseases." In: **Nat Neurosci** 21.10 (Oct. 2018), pp. 1341–1349. doi: 10.1038/s41593-018-0238-6.
4. A. Raj, A. Kucyeski, and M. Weiner. "A network diffusion model of disease progression in dementia." In: **Neuron** 73.6 (Mar. 2012), pp. 1204–1215. doi: 10.1016/j.neuron.2011.12.040.
5. C. Mezas and A. Raj. "Analysis of Amyloid- $\beta$  Pathology Spread in Mouse Models Suggests Spread Is Driven by Spatial Proximity, Not Connectivity." In: **Front Neurol** 8 (2017), p. 653. doi: 10.3389/fneur.2017.00653.



6. C. Mezas, E. LoCastro, C. Xia, and A. Raj. "Connectivity, not region-intrinsic properties, predicts regional vulnerability to progressive tau pathology in mouse models of disease." In: **Acta Neuropathol Commun** 5.1 (Aug. 2017), p. 61. doi: 10.1186/s40478-017-0459-z.
7. M. X. Henderson, E. J. Cornblath, A. Darwich, B. Zhang, H. Brown, R. J. Gathagan, R. M. Sandler, D. S. Bassett, J. Q. Trojanowski, and V. M. Y. Lee. "Spread of  $\alpha$ -synuclein pathology through the brain connectome is modulated by selective vulnerability and predicted by network analysis." In: **Nat Neurosci** 22.8 (Aug. 2019), pp. 1248–1257. doi: 10.1038/s41593-019-0457-5.
8. O. Sporns. "Graph theory methods: applications in brain networks." In: **Dialogues Clin Neurosci** 20.2 (June 2018), pp. 111–121. doi: 10.31887/DCNS.2018.20.2/osporns.
9. S. W. Oh et al. "A mesoscale connectome of the mouse brain." In: **Nature** 508.7495 (Apr. 2014), pp. 207–214. doi: 10.1038/nature13186.
10. K. C. Luk, V. Kehm, J. Carroll, B. Zhang, P. O'Brien, J. Q. Trojanowski, and V. M. Lee. "Pathological  $\alpha$ -synuclein transmission initiates Parkinson-like neurodegeneration in nontransgenic mice." In: **Science** 338.6109 (Nov. 2012), pp. 949–953. doi: 10.1126/science.1227157.
11. P. Pandya, C. Mezas, and A. Raj. "Predictive Model of Spread of Progressive Supranuclear Palsy Using Directional Network Diffusion." In: **Front Neurol** 8 (Dec. 2017), p. 692. doi: 10.3389/fneur.2017.00692.
12. H. Fu, J. Hardy, and K. E. Duff. "Selective vulnerability in neurodegenerative diseases." In: **Nat Neurosci** 21.10 (Oct. 2018), pp. 1350–1358.
13. F. Claudi, A. L. Tyson, L. Petrucco, T. W. Margrie, R. Portugues, and T. Branco. "Visualizing anatomically registered data with Brainrender." In: **eLife** 10 (Mar. 2021). doi: 10.7554/elife.65751.
14. N. L. Rey, J. A. Steiner, N. Maroof, K. C. Luk, Z. Madaj, J. Q. Trojanowski, V. M.-Y. Lee, and P. Brundin. "Widespread transneuronal propagation of alpha-synucleinopathy triggered in olfactory bulb mimics prodromal Parkinson's disease." In: **Journal of Experimental Medicine** 213.9 (Aug. 2016), pp. 1759–1778. doi: 10.1084/jem.20160368.
15. A. Recasens et al. "Lewy body extracts from Parkinson disease brains trigger  $\alpha$ -synuclein pathology and neurodegeneration in mice and monkeys." In: **Ann Neurol** 75.3 (Mar. 2014), pp. 351–362.
16. M. Bourdenx et al. "Identification of distinct pathological signatures induced by patient-derived  $\alpha$ -synuclein structures in nonhuman primates." In: **Sci Adv** 6.20 (May 2020), eaaz9165.
17. A. Raj and F. Powell. "Models of Network Spread and Network Degeneration in Brain Disorders." In: **Biological Psychiatry: Cognitive Neuroscience and Neuroimaging** 3.9 (Sept. 2018), pp. 788–797. doi: 10.1016/j.bpsc.2018.07.012.